

Privacy-Preserving Visual Localization with Event Cameras

Junho Kim^{1*} Young Min Kim¹ Yicheng Wu² Ramzi Zahreddine²
Weston A. Welge² Gurunandan Krishnan² Sizhuo Ma^{2†} Jian Wang^{2†}

¹Seoul National University ²Snap Inc.

Abstract

We present a robust, privacy-preserving visual localization algorithm using event cameras. While event cameras can potentially make robust localization due to high dynamic range and small motion blur, the sensors exhibit large domain gaps making it difficult to directly apply conventional image-based localization algorithms. To mitigate the gap, we propose applying event-to-image conversion prior to localization which leads to stable localization. In the privacy perspective, event cameras capture only a fraction of visual information compared to normal cameras, and thus can naturally hide sensitive visual details. To further enhance the privacy protection in our event-based pipeline, we introduce privacy protection at two levels, namely sensor and network level. Sensor level protection aims at hiding facial details with lightweight filtering while network level protection targets hiding the entire user's view in private scene applications using a novel neural network inference pipeline. Both levels of protection involve light-weight computation and incur only a small performance loss. We thus project our method to serve as a building block for practical location-based services using event cameras. The code and dataset will be made public through the following link: https://82magnolia.github.io/event_localization/.

1. Introduction

Visual localization is a versatile localization method widely used in AR/VR that aims to find the camera pose only using image input. While recent visual localization methods successfully provide robust camera pose estimation in a variety of scenes [54, 64, 67, 71], privacy concerns may arise due to the requirement of image capture for localization [10, 12]. As shown in Figure 1, the localization service user may be concerned with sharing the current view

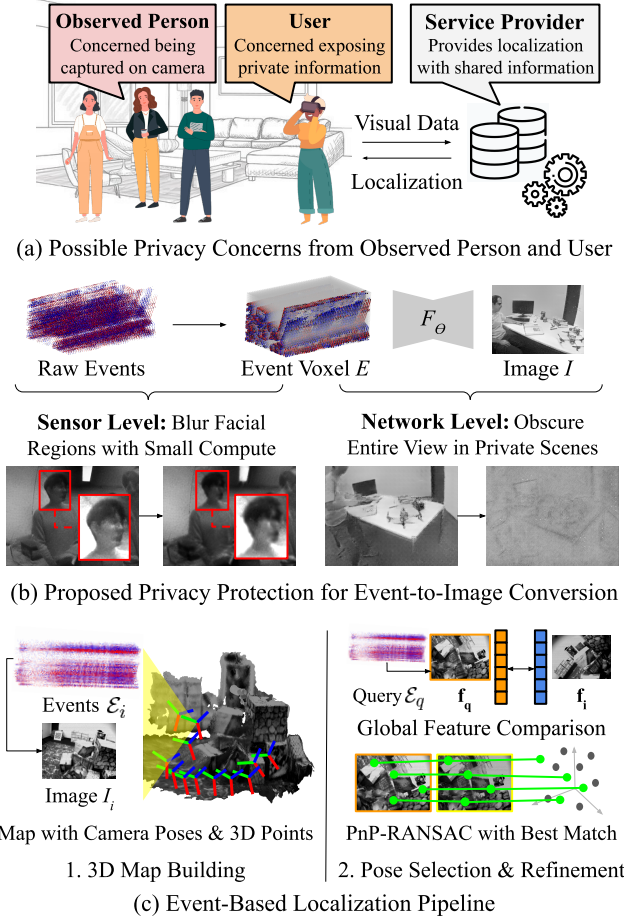


Figure 1. Overview of our approach. We target concerns in client-server localization where the user with limited compute shares visual information with the service provider. Our privacy protection operates at sensor and network level, which enables hiding sensitive details for event-to-image conversion. The results are then used for our localization pipeline which involves converting events to images and applying image-based localization.

with the service provider, which is inevitable in edge devices with a limited amount of compute (e.g. smartphones, AR glasses). Further concerns can arise in the observed

*Work done during an internship at Snap Research

†Co-corresponding authors

person side, who can be unknowingly captured in the localization process of another person’s camera. This concern in particular has been widely addressed in mobile applications by notifying when camera capture is happening [1, 4, 5], but mere notification is insufficient to fully alleviate the concerns of observed people.

Event cameras, which are visual sensors that only record brightness changes [19, 39], have the potential to provide robust, privacy-preserving visual localization. Unlike normal cameras that capture the absolute scene brightness, these cameras encode brightness changes as a stream of events. The sensors have a high temporal resolution and dynamic range, which is beneficial for robust localization in challenging scenarios such as low lighting or fast camera motion. Further, as the power consumption of the sensor is far lower than normal cameras [19], performing machine vision using these sensors is amenable for applications in AR/VR. In a privacy perspective, since only a fraction of visual information is captured, the sensors can naturally hide fine-grained visual details at the expense of relatively unstable visual features compared to normal cameras.

We propose an event-based visual localization method that can perform robust localization while preserving privacy. Our proposed scenario assumes a light-weight capture and computation from the user side and heavy processing from the service provider side. For localization, we employ event-to-image conversion to adapt powerful image-based localization methods [24, 51, 53] on the data captured from an edge device equipped with an event camera. Here the service provider performs the computationally expensive conversion [49, 56, 57, 63, 68] and applies visual localization on the recovered image. Our resulting pipeline inherits the advantages of event cameras and state-of-the-art image features [14, 52]: we can perform stable and accurate localization in fast camera motion or low lighting, where visual localization using normal cameras typically fails.

We additionally integrate privacy protection specifically tailored for event cameras in two levels, namely sensor level and network level as shown in Figure 1b. In the sensor level, we propose a novel filtering method that blurs facial landmarks without explicitly detecting them, while preserving important landmarks for localization as shown in Figure 4. This process reduces people’s concern about being recorded by edge device users, and is sufficiently light-weight for implementation on sensor chips. In the network level, we propose to split neural network inference during localization so that the costly intermediate computation is performed on the service provider side, while simultaneously preventing the service provider from reconstructing images from events. The technique targets users willing to use location-based services in private spaces (e.g. apartment rooms), where hiding the entire user view may be solicited as shown in Figure 4. Both levels of privacy protection are light-weight and

incur only a small drop in localization performance, which are further verified in our experiments.

We evaluate our method on a wide range of localization scenarios including scenes captured with moving people, low-lighting, or fast camera motion. Experiments show that our approach can robustly localize in such challenging scenarios and the privacy protection pipeline can effectively hide sensitive visual content while preserving localization performance. As our task is fairly new, we record new datasets called EvRooms and EvHumans which will be partially released in public to spur further research in event-based visual localization. To summarize, our key contributions are: (i) robust localization in challenging conditions using event cameras, (ii) sensor level privacy protection for relieving observed people’s concerns, and (iii) network level privacy protection for mitigating user’s concerns. Equipped with robust localization and privacy protection, we expect our method to offer a practical solution to camera pose estimation using event cameras.

2. Related Work

Event-Based Mapping and Localization Due to the high dynamic range and small motion blur, event cameras are suitable for visual odometry (VO) or SLAM tasks involving sequential pose estimation and depth prediction. Existing works in this direction [9, 20, 23, 27, 31, 32] propose various event aggregation and measurement update methods to effectively utilize event data with minimal latency. Based on the findings from event-based VO and SLAM literature, recent works leverage event cameras for novel view synthesis [26, 35, 50] where the hardware-level benefits enable view synthesis robust to low lighting or motion blur.

However, re-localizing an event camera with respect to a pre-built 3D map, namely event-based visual localization, is a fairly understudied problem. Prior works perform direct camera pose estimation using neural networks [28, 46]. While these methods can quickly localize with a single neural network inference, the networks should be separately trained for each test scene. Also, it is widely known in image-based localization that structure-based methods outperform direct methods [30, 55, 67]. These methods leverage correspondences in 2D and 3D by comparing feature descriptors [7, 14, 25, 51–53]. We employ the structure-based paradigm on event cameras, leading to stable localization while also benefiting from the sensor-level strengths.

Privacy-Preserving Machine Vision As many machine vision applications take the entire image view as input, privacy breaches could occur [10, 12]. Recent works propose to apply additional transformations on the input image data [16, 36, 70] to hide the user identity, or encrypt the visual data in the sensor level by incorporating specially designed optics [48, 65, 66, 72]. Many prior works

in privacy-preserving visual localization follow the former approach, where existing methods suggest lifting the 2D, 3D keypoints to lines [21, 61, 62], or training a new set of feature descriptors hiding sensitive details [12, 15, 45]. Our method takes a hybrid approach, where we propose to use event cameras as privacy-preserving sensors for localization and apply dedicated transformations on the event data to hide sensitive visual details.

3. Event-Based Localization Pipeline

Given a short stream of events recorded by an event camera, our method aims to find the 6DoF camera pose within a 3D map as shown in Figure 1. Event cameras are visual sensors that track brightness changes as a stream of events, $\mathcal{E} = \{e_i = (x_i, y_i, t_i, p_i)\}$, where e_i indicates the brightness change of polarity $p_i \in \{+1, -1\}$ at pixel location (x_i, y_i) and timestamp t_i .

Our localization method utilizes images reconstructed from voxelized events. Given an input event stream \mathcal{E} , let E denote the event voxel grid [49, 57, 75] obtained by taking weighted sums of event polarities within spatio-temporal bins. Event-to-image conversion methods [42, 49, 57, 63, 68] take the event voxels as input and produce images using neural networks, namely $F_\Theta(E) = I$ where Θ denotes the neural network parameters. Below we describe the steps taken by our method to perform event-based localization.

Structure-Based Localization Figure 1c shows our localization process. Given event streams from a scene $S_e = \{\mathcal{E}_1, \dots, \mathcal{E}_N\}$ with each stream spanning a short time, we first convert events into images $S_i = \{I_1, \dots, I_N\}$. Then we run the off-the-shelf structure-from-motion pipeline COLMAP [58] on S_i . The result is a map containing 3D points and 6DoF pose-annotated images.

As the next step, we use global features vectors from NetVLAD [7] for candidate pose selection. Given a captured query event stream \mathcal{E}_q , we first reconstruct the image I_q and extract its NetVLAD feature vector $\mathbf{f}_q \in R^{4096}$. Similarly, for each pose-annotated reference image I_i in the 3D map, we extract its feature vector \mathbf{f}_i . We compute the L2 distances between the query and reference image features and select the top-K nearest poses for further refinement.

Finally, for refinement, we first perform local feature matching [14, 52] between the query and selected reference images. We count the number of matches found for each query-reference pair and choose the reference view I_r with the largest number of matches. Then we obtain the refined 6DoF pose by retrieving the 3D points visible from I_r and performing PnP-RANSAC [18, 22, 37, 38] between the 2D points in I_q and retrieved 3D points.

By leveraging event-to-image conversion, we can effectively deploy powerful image-based localization methods on events. Nevertheless, for high-quality image recov-

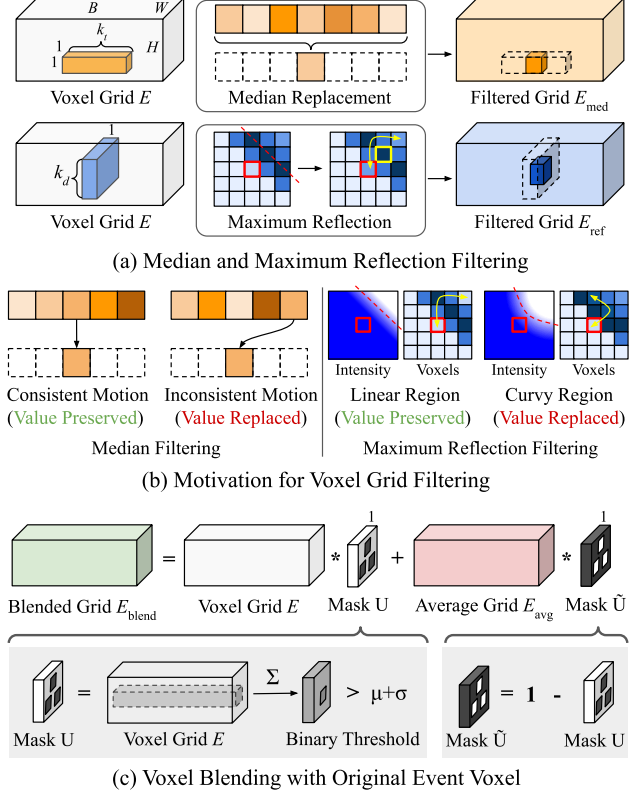


Figure 2. Sensor-level privacy protection. We attenuate temporally inconsistent regions via median filtering and curvy regions via maximum reflection filtering. To reduce artifacts, the averaged voxels $E_{avg} = (E_{med} + E_{ref})/2$ are blended with the original voxels.

ery the conversion solicits repetitive neural network inferences [49, 63], which can be costly for edge devices. This necessitates the transmission of visual information from edge devices to service providers, where we propose various techniques for preserving privacy in Section 4.

4. Privacy-Preserving Localization

In this section, we describe the procedures for privacy preservation. As in Figure 1, we consider the case where the localization service user, equipped with an edge device, has limited computing power and shares the visual information with the service provider. We propose two levels of privacy protection to prevent possible breaches during information sharing. **Sensor-level privacy protection** focuses on hiding facial details and could be easily applied with small additional computations. **Network-level privacy protection** targets localization in private scenes, where the user would want to completely hide what they are looking at.

4.1. Sensor-Level Privacy Protection

Sensor-level privacy protection removes temporally inconsistent or curvy regions and blends the result with the

original voxel. This low-level operation preserves static structure while blurring out dynamic or facial information.

Median Filtering We first filter temporally inconsistent regions via median filtering along the temporal axis as shown in Figure 2a. Given a voxel grid $E \in \mathbb{R}^{B \times H \times W}$ where B denotes the number of temporal bins and H, W denote the height and width of the sensor resolution, we replace each voxel $E(l, m, n)$ with the median value from $E(l - k_t : l + k_t, m, n)$ where k_t is the temporal window size. Since dynamic entities, including human faces, may deform over time, the resulting voxel regions will show irregularities in the temporal domain. Median filtering perturbs voxel entries with temporally inconsistent intensity or motion as shown in Figure 2b, where detailed expositions on this notion are given in the supplementary material. As a result, events from faces after filtering lead to low quality image reconstructions.

Maximum-Reflection Filtering We propose maximum-reflection filtering on the spatial domain to attenuate event accumulations from curvy regions. For each voxel $E(l, m, n)$ we first find the location (l, m^*, n^*) that attains the maximum event count within the spatial neighborhood $|E(l, m - k_s : m + k_s, n - k_s : n + k_s)|$, where k_s is the spatial window size. We then replace $E(l, m, n)$ as the voxel value at the reflected location with respect to (l, m^*, n^*) , namely $E(l, 2m^* - m, 2n^* - n)$. The maximum-reflection filtering preserves event accumulation near lines while replacing other regions with arbitrary values. As shown in Figure 2b, if the original intensities follow a step function event accumulations near lines are symmetrical with respect to the local maximum. Although lines from real-world scenes are not strictly a step function, we find that in practice, the maximum-reflection filtering can well-preserve events near lines while attenuating other regions including faces.

Voxel Blending For voxel grid regions with an insufficient amount of accumulations, the filtering process can incur artifacts as the signal-to-noise ratio is low. Therefore, we blend the filtered voxels with the original event voxel using binary thresholding as depicted in Figure 2b. To elaborate, the binary mask $U \in \mathbb{R}^{B \times H \times W}$ is defined as follows,

$$U(l, m, n) = \begin{cases} 1 & \text{if } \sum_i |E(i, m, n)| > \mu + \sigma \\ 0 & \text{otherwise,} \end{cases} \quad (1)$$

where μ, σ is the mean and standard deviation of the temporally-summed event accumulations, $\sum_l |E(l, m, n)|$. Then, the blended voxel is given as

$$E_{\text{blend}} = U \cdot \left(\frac{E_{\text{med}} + E_{\text{max}}}{2} \right) + (1 - U) \cdot E, \quad (2)$$

where $E_{\text{med}}, E_{\text{max}}$ denote the median and maximum-reflection filtered voxels respectively.

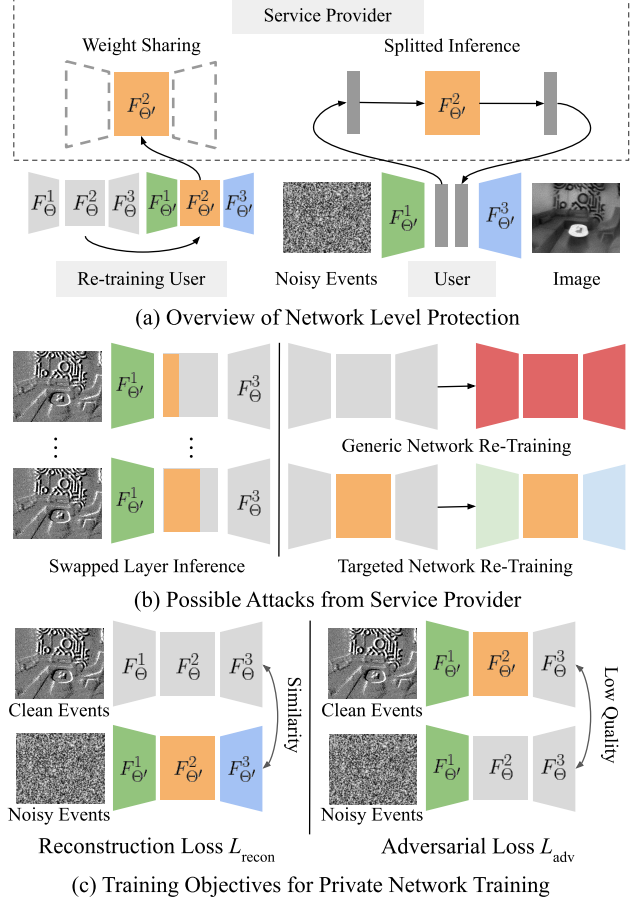


Figure 3. Network level privacy protection targeting users in private scenes. To save compute while hiding sensitive visual information, the inference is split between the user and service provider where the users deploy a privately-trained reconstruction network $F_{\Theta'}$. The network is trained using special loss functions and noise-infused event voxels to prevent possible attacks from the service provider to reconstruct images using shared information.

4.2. Network-Level Privacy Protection

As shown in Figure 1, network level privacy protection completely hides the user's view from the service provider in private spaces while saving user-side compute. Here we suggest splitting the event-to-image conversion process between the service provider and user, where the inference is done with a privately re-trained reconstruction network $F_{\Theta'}$. We retain our focus on making the event-to-image conversion process privacy-preserving, as once the images are securely reconstructed one can apply existing privacy-preserving visual localization methods [15, 45, 61, 62] to find the camera pose.

Splitted Inference and Possible Attacks The entire splitted inference process is summarized in Figure 3a. Prior to inference, the users re-train a private version of the conversion network $F_{\Theta'}$. The network learns to reconstruct im-

ages from noise-infused voxel grids $\tilde{E}=E+E_{\text{noise}}$ where the noise E_{noise} is fixed for each private scene and unknown to the service provider. We describe the detailed training process in the preceding paragraphs. After training, the users divide the network to three parts $F_{\Theta'}^1, F_{\Theta'}^2, F_{\Theta'}^3$, where $F_{\Theta'}^2$ contains the majority of the inference computation and is *the only shared part* with the service provider. During inference, (i) the user performs inference on $F_{\Theta'}^1$ using the noise-infused voxel grid \tilde{E} , (ii) the result is sent to the service provider to perform $F_{\Theta'}^2$, and (iii) the user retrieves the result to finally perform $F_{\Theta'}^3$. Since the frontal and rear inference is done on-device, we can make the conversion process privacy preserving if the service provider cannot ‘eavesdrop’ on the intermediate inference results.

As shown in Figure 3b, we have identified three possible attacks from the service provider: swapped layer inference, generic network re-training, and targeted network re-training. First, in *swapped layer inference* one takes the intermediate inference results made with Θ' and runs the rest of the reconstruction using the original network parameters Θ . The other two attacks involve re-training a new set of networks using large amounts of event data presumably available to the service provider. *Generic network re-training* trains a randomly initialized neural network using the same training objectives as in the private training. *Targeted network re-training* similarly trains a neural network using the same objectives, but initializes the intermediate parts of the network with the shared parameter values from $F_{\Theta'}^2$. Using the re-trained networks, the service provider could try swapped layer inference as shown in Figure 3b.

Private Network Training for Attack Prevention To prevent possible attacks, we propose a novel training process usable by any person within the private space to obtain a new set of event-to-image conversion network $F_{\Theta'}$. Here the training starts from random weight initialization and is quickly done using a small amount of event data captured within the private space. The trained network is then shared between the trusted parties in the private space as shown in Figure 3a.

During training, we impose the new network to learn the reconstruction from the original network F_{Θ} while taking a fixed noise E_{noise} as additional input. This obfuscates the network weights learned from training and prevents the service provider from reverse-engineering the trained results, namely *generic/targeted network re-training attacks*.

For training we impose two losses $L=L_{\text{recon}}+L_{\text{adv}}$, where L_{recon} , L_{adv} are the reconstruction and adversarial losses respectively. Formally, the reconstruction loss is given as follows,

$$L_{\text{recon}} = d(F_{\Theta}(E), F_{\Theta'}(\tilde{E})), \quad (3)$$

where $d(\cdot, \cdot)$ is the LPIPS distance [74] and $\tilde{E}=E+E_{\text{noise}}$ is

the noise-infused event voxel.

The adversarial loss enforces the new network weights to deviate from the original network F_{Θ} , which in turn offers prevention against *swapped layer inference attacks*. We first split the neural network into three parts $F_{\Theta}^1, F_{\Theta}^2, F_{\Theta}^3$ where each part corresponds to the frontal, middle, and rear parts of the network. As shown in Figure 3a, the loss is defined as the sharpness of the image reconstructions made by swapping parts of the new network layers with the original weights,

$$L_{\text{adv}} = s(F_{\Theta}^3 \circ F_{\Theta}^2 \circ F_{\Theta'}^1(\tilde{E})) + s(F_{\Theta}^3 \circ F_{\Theta'}^2 \circ F_{\Theta}^1(\tilde{E})), \quad (4)$$

where $s(\cdot)$ is the average image sharpness calculated by applying Sobel filters [29] on the reconstructions.

5. Experiments

We first validate our choice of the event-based localization pipeline in Section 5.1 and further validate the two privacy protection methods in Section 5.2.

Dataset and Implementation Details We use three datasets for evaluation: DAVIS240C [43], EvRooms, and EvHumans. DAVIS240C consists of scenes captured using the DAVIS camera [8] which simultaneously outputs events and frames. We use six scenes from the dataset that are suitable for localization. EvRooms is a newly collected dataset to evaluate the robustness of event-based localization algorithms amidst challenging external conditions. The dataset is captured in 20 scenes and divided into recordings containing fast camera motion (EvRooms^F) and low lighting (EvRooms^L). EvHumans is another newly collected dataset for evaluating privacy-preserving localization amidst moving people. The dataset is captured with 22 volunteers moving in 12 scenes. Both datasets are captured using the DAVIS346 [2] camera. Additional details on dataset preparation are deferred to the supplementary material.

In all our experiments we use the RTX 2080 GPU and Intel Core i7-7500U CPU. For event-to-image conversion, we adopt E2VID [49], which is a conversion method widely used in event-based vision applications [17, 44]. Unless specified otherwise, we use $K=3$ candidate poses for refinement in our localization pipeline from Section 3. For results reporting accuracy, a prediction is considered correct if the translation error is below 0.1 m and the rotation error is below 5.0°. All translation and rotation values are median values, following [33, 51, 53].

5.1. Localization Performance Analysis

Event-Based Localization Comparison We use the DAVIS240C dataset [43] for evaluation, and consider six baselines: direct methods (PoseNet [30], SP-LSTM [46]), and structure-based methods taking various event representations as input (binary event image [11], event his-

Method	Description	t -error (m)	R -error ($^{\circ}$)	Acc.
Direct	PoseNet [30]	0.15	15.94	0.05
	SP-LSTM [46]	0.19	20.30	0.03
Structure-Based	Binary Event Image [11]	0.07	3.77	0.54
	Event Histogram [41]	0.06	3.02	0.62
	Timestamp Image [47]	0.06	3.18	0.58
	Sorted Timestamp Image [6]	0.06	3.19	0.59
Ours	Event-to-Image Conversion	0.05	2.06	0.72

(a) Event-Based Localization Comparison

Dataset Split	Method	t -error (m)	R -error ($^{\circ}$)	Acc.
Normal	Image-Based	0.04	1.77	0.72
	Event-Based	0.05	2.00	0.73
Low Lighting	Image-Based	0.26	10.90	0.26
	Event-Based	0.05	2.53	0.68
Fast Motion	Image-Based	0.18	6.25	0.26
	Event-Based	0.05	1.82	0.72

(b) Image-Based Localization Comparison

Table 1. Localization evaluation against existing methods.

togram [41, 69], timestamp image [47], and sorted timestamp image [6]). We provide detailed explanations about the baselines in the supplementary material.

Table 1a shows the localization results of our method and the baselines. All structure-based methods outperform direct methods, as the pose refinement step using PnP-RANSAC [18, 38] enables accurate localization. Among the structure-based methods, our method outperforms the baselines by a large margin as the event-to-image conversion mitigates the domain gap and allows our method to fully leverage the robustness of image feature descriptors [7, 14].

Image-Based Localization Comparison We implement an exemplary image-based localization method by replacing the input modality in our pipeline from events to images. We create three splits from DAVIS240C and EvRooms based on the target scenario: normal, low lighting, and fast motion. Normal consists of four scenes from DAVIS240C recorded in slow camera motion and average lighting. The other two splits are more challenging, with (i) low lighting containing two scenes from DAVIS240C and EvRooms^L recorded in low lighting, and (ii) fast motion containing EvRooms^F captured with fast motion.

Table 1b compares localization results under various settings. The performance of the two methods are on par in the normal split, as image-based localization can confidently extract good global/local features in benevolent conditions. However, the performance gap largely increases in the low lighting, and fast motion splits, as the motion blur and low exposure make feature extraction difficult. Due to the high dynamic range and temporal resolution of event cameras, our method can perform robust localization even in these challenging conditions.

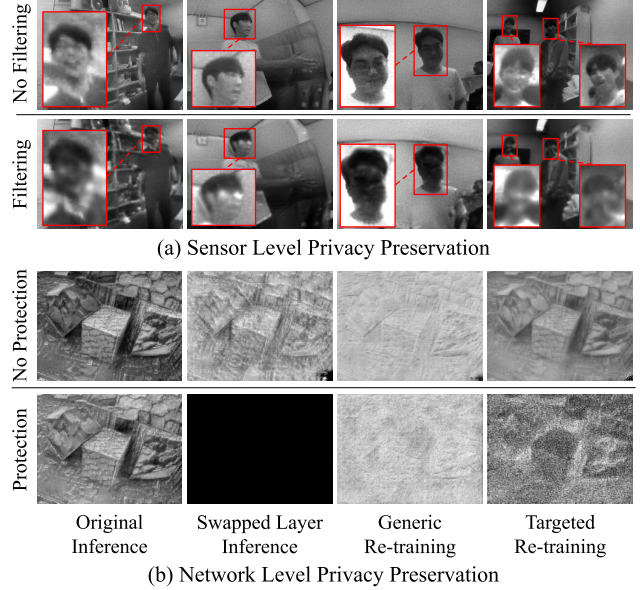


Figure 4. Qualitative results of privacy protection.

5.2. Privacy Preservation Evaluation

5.2.1 Sensor Level Privacy Protection

We use the EvHumans dataset to assess how the sensor level protection can hide facial landmarks. In all experiments, we set the spatial/temporal window size as $k_s=23$, $k_t=13$. Other details on the sensor-level protection evaluation is reported in the supplementary material.

Face Blurring Assessment We examine face blurring in terms of low-level image characteristics and high-level semantics. For evaluation, we generate 9,755 image reconstruction pairs from the event streams with/without sensor level protection. Also, we use the publicly available FaceNet [3] and DeepFace [59, 60] libraries for high-level evaluation.

Table 2b reports the average sharpness of the faces detected from the reconstructed images. For a fair comparison, we first run face detection on the non-filtered image reconstruction and use the detection results to crop both filtered/non-filtered versions. The sharpness largely drops after filtering, which indicates that our sensor level protection can effectively blur facial landmarks. Table 2c further supports this claim, where we measure the image similarity between the two image reconstructions separately for facial and background regions. The similarity metrics are much higher for background regions, meaning that our method can keep important localization cues ample in the background while blurring out faces. Some exemplary results are shown in Figure 4a, where the faces are blurred out from filtering while the background features remain intact.

For high-level analysis, Table 2b reports the face detec-

Method	t -error	R -error	Acc.	# of Faces	Sharpness	Re-ID Acc.
No Protection	0.04	0.99	0.84	1034	0.0956	0.9387
Protection	0.05	1.28	0.73	192	0.0475	0.5377

(a) Localization and Face Protection Evaluation

Region	PSNR (\downarrow)	SSIM (\downarrow)	MAE (\uparrow)
Face	18.1620	0.3572	0.1974
Background	21.1243	0.6677	0.1391

(b) Reconstruction Quality after Protection

Table 2. Sensor Level Privacy Preservation Evaluation.

Method	t -error	R -error	Acc.	# of Faces	Sharpness	Re-ID Acc.
w/o Blending	0.06	1.61	0.64	106	0.0286	0.4670
w/o Max Reflection	0.05	1.17	0.77	354	0.0483	0.5708
w/o Median Filtering	0.05	1.23	0.75	231	0.0461	0.5613
Ours	0.05	1.28	0.73	192	0.0475	0.5377

Table 3. Ablation study on sensor level protection.

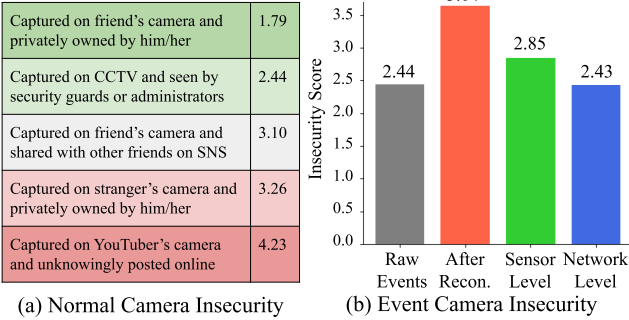


Figure 5. User study results. The insecurity scores range between 1 and 5. We make an initial measurement on how users feel about being captured using normal cameras in various scenarios. Then, we query about event cameras by sequentially showing raw events, event-to-image reconstructions, and privacy protection results.

tion and grouped face re-identification results. We apply a face detection algorithm [73] on the image reconstructions, where the number of detected faces largely decreases after filtering. Note however that even without filtering, the number of faces detected is fairly small ($\sim 1,000$) given that on average two faces are present for the $\sim 10,000$ test images. As event cameras only capture a fraction of visual data, it can naturally offer a minimal level of face blurring, which could also be verified from the reconstructions in Figure 4. We further analyze how the filtering obfuscates facial features with grouped face re-identification. In this task, we first divide the faces of volunteers in EvHumans to disjoint groups and apply face re-identification [13] on the detected faces to check whether it belongs to a certain group or not. Additional details regarding the task are explained in the supplementary material. Similar to face detection, re-identification accuracy largely drops after filtering, indicating the efficacy of our method to obfuscate facial semantics.

User Study Along with the low-level and high-level analysis, we conduct a user study to examine how the actual users would feel about our face blurring. We request 39 volunteers to answer a survey that assesses how insecure people feel about various capturing scenarios, where the insecurity is scored from 1 to 5. As shown in Figure 5a, the survey makes an initial assessment of being captured with normal cameras for situations such as tourist spots and CCTV. Then the survey evaluates event cameras in three steps: the users first observe raw event measurements, then the image reconstructions from events, and finally the image reconstructions after sensor level protection. We share the details about the survey along with the detailed answers of the subjects in the supplementary material.

Figure 5 displays the survey results. In the initial assessment from Figure 5a, people have varying levels of insecurity depending on the capturing scenario and the results give a rough translation between the insecurity scores in the follow-up questions using event cameras. In Figure 5b, the subjects first give a low insecurity score when they see the raw events but increase their score once they observe that image reconstruction is possible. The scores drop after people observe the face blurring, to a level roughly equivalent to 'being captured on CCTV / friend's camera'. The results show that our method can indeed alleviate the concerns presented by users when using AR/VR services.

Localization Evaluation and Ablation Study We evaluate localization while using sensor level protection, where we pass the filtered voxels to our main localization pipeline. As shown in Table 2a, only a small drop in accuracy occurs. While attenuating facial features, sensor level protection can preserve important features for localization.

We finally perform an ablation study on the key components of sensor level protection. As shown in Table 3, using the two filters along with voxel blending makes an optimal trade-off between privacy protection and localization performance. If we ablate the median or max reflection filters, the number of detected faces increases which indicates that the faces are less protected. However, if we ablate voxel blending, the localization accuracy drastically decreases. Each component in the sensor level protection is necessary for effective privacy-preserving localization.

5.2.2 Network Level Privacy Preservation

We use the six scenes from the DAVIS240C dataset to evaluate how network level protection can hide scene details in private spaces. For each scene, we re-train an event-to-image conversion network following the procedure from Section 4.2. The re-training is quickly done using Adam [34] with learning rate $1e-4$ and batch size 2 for 10 epochs. Then for each trained model, we perform generic and targeted network re-training, where the models are trained using events generated from MS-COCO [40]

following [49, 57]. During inference, from the E2VID [49] architecture we use the first two layers as the frontal part ($F_{\Theta'}^1$), the last two layers as the rear part ($F_{\Theta'}^3$), and the rest as the middle part ($F_{\Theta'}^2$). Additional details about the evaluation is deferred to the supplementary material.

Attack Protection Assessment and User Study We first assess how our method can prevent possible attacks (swapped layer inference, generic/targeted network re-training) from the service provider to recover images using the shared visual information. For each attack type, we simulate the procedure from Section 4.2 by performing image reconstruction where the frontal part of the inference uses the client’s network $F_{\Theta'}$ and the latter part uses the service provider’s network. The splitting is done at various locations in the network, and we show in Table 4 the averaged similarity metrics between the attacks and the reconstructions from the original network F_{Θ} . The full results are reported in the supplementary material.

As shown in Table 4, the reconstruction quality after network level protection is constantly low for all three attack scenarios. The adversarial loss (Equation 4) plays a key role in blocking swapped layer inference (‘ours’ vs ‘ours w/o adversarial loss’). Simply re-training with random initialization offers a defense against generic network re-training, as all the methods constantly show large image deviations. For targeted network re-training, a large similarity gap occurs from applying noise watermarking (‘ours’ vs ‘ours w/o noise watermarking’) which indicates the crucial role of this procedure for preventing the attack. We show exemplary visualizations of the three attacks in Figure 4, where all attacks fail after network level protection.

Finally, we conduct a user study to see how people feel about the network level protection. Here we survey 23 volunteers using a questionnaire similar to the sensor level evaluation, but with an additional question in the end showing image reconstructions from network level protection. Figure 5 displays the results, where the insecurity score is lower than the sensor level privacy protection. While the network level protection requires additional re-training, it can offer an added layer of privacy preservation compared to the sensor level method as the entire view is obscured.

Compute Efficiency and Localization Assessment In addition to privacy protection, network level protection reduces the computational burden of running the entire event-to-image conversion on-device. To assess the computational efficiency, we compare the inference runtime on CPU, GPU, and our method that performs splitting between the two. Here the CPU and GPU are used to model the edge device and service provider respectively. As shown in Table 4, the runtime of our method is significantly lower than only using CPU, and comparable to the case only using GPU. While the results may differ from the actual run-

Method	t -error (m)	R -error (°)	Acc.
No Protection	0.04	2.29	0.69
Sensor Level Protection	0.05	2.50	0.66
Network Level Protection	0.05	2.58	0.64
Joint Protection	0.06	2.88	0.62

(a) Localization Evaluation Including Joint Protection

Attack Type	Swapped Layer Inference	Generic Re-Training	Targeted Re-Training
Random Initialization	0.4613	0.4579	0.2165
Ours w/o Noise Watermark	0.9760	0.4249	0.3237
Ours w/o Adversarial Loss	0.4746	0.4456	0.3517
Ours	0.9587	0.4492	0.4415

(b) Reconstruction Quality (MAE) of Possible Attacks

Method	Pure CPU	Pure GPU	Splitted (Ours)
Runtime (s)	0.8239	0.0119	0.0760

(c) Runtime Comparison

Table 4. Network level privacy preservation evaluation.

time characteristics of edge devices and service providers, our method can efficiently distribute the computation and reduce the burden on the edge device side.

We further evaluate the localization performance while using network level protection. Here we use the re-trained network for image reconstruction in our localization pipeline. Note it is also possible to apply any other privacy-preserving image-based localization methods [12, 15, 45, 61, 62] on the securely reconstructed images. Similar to sensor level protection, accuracy only drops mildly as shown in Table 3. Our network level protection offers secure image reconstruction while enabling stable localization.

Joint Sensor and Network Level Protection While network level protection hides the visual content from the service provider, residents in private spaces may still feel uncomfortable about being captured. To this end, in Table 4a we evaluate the localization performance using both protection methods. Only a small performance decrease occurs even when applying both levels of protection. Thus our method can handle a wide variety of privacy concerns, while not significantly sacrificing the utility of localization.

6. Conclusion and Future Work

We proposed a robust event-based localization algorithm that can simultaneously protect user privacy. Our method exploits event-to-image conversion to adapt structure-based localization on event cameras for robust localization. To protect privacy during the conversion, we propose sensor and network level protection. Sensor level protection targets hiding facial landmarks, whereas network level protection aims to hide the entire view for users in private scenes. Both levels of protection are light-weight, and our experiments show that the protections incur only small performance drops. We expect our method to be used as a prac-

tical pipeline for event-based machine vision systems and further spur research in localization using event cameras.

We observe two key limitations of our method that solicits future work. First, some participants in our user study suggested that deleting faces in sensor level protection may be insufficient as people could be identified from other signals such as unique gestures or body features. Developing a privacy protection method that hides a wider range of features will be an interesting direction. Another limitation is that network level privacy protection could only be used in a fixed private scene. Investigating re-training methods for networks to hide the user’s view while reliably reconstructing images in the wild will be another promising direction.

A. Method Details

A.1. Sensor Level Protection

Accelerating Filtering To blur regions possibly containing facial landmarks, sensor level privacy protection applies median and maximum reflection filtering on the event voxel grid followed by voxel blending (Section 4.1). We reduce the runtime of sensor level protection by exploiting the fact that the blending process only keeps the filtered values for pixels with sufficient number of event accumulations. Namely, we sparsely apply the filtering operation only on the pixel regions where the binary mask in Equation 1 is non-zero. This simple optimization reduces the runtime from 4.32 s to 0.15 s for processing 3×10^5 events spanning approximately 0.45 s. Note that the runtime is measured from filters implemented using pure Python code, and the process could be further accelerated by re-implementing the filters with faster languages such as C++. Nevertheless, sparsely applying filtering leads to a large amount ($\sim 30\times$) of runtime acceleration.

Justification of Median Filtering Among the two voxel filtering steps, median filtering attenuates temporally inconsistent voxel regions. Here we give a mathematical justification of median filtering based on the event generation equation [19]. First, let $L(\mathbf{u}, t)$ denote the log intensity at pixel \mathbf{u} in time t . Then, assuming constant illumination and motion, we can write the event accumulation from a short time interval $[t - \Delta t, t]$ as follows [19],

$$\Delta L(\mathbf{u}, t) = \nabla L(\mathbf{u}, t) \cdot \mathbf{v} \Delta t, \quad (5)$$

where \mathbf{v} is the pixel velocity. Similarly, the event accumulations over a short time Δt for the neighboring timestamps $t \pm \Delta t$ could be expressed as $\Delta L(\mathbf{u}, t \pm \Delta t) = \nabla L(\mathbf{u}, t \pm \Delta t) \cdot \mathbf{v} \Delta t$. Using Taylor expansion and the constant velocity/illumination assumption, we have

$$L(\mathbf{u}, t \pm \Delta t) = L(\mathbf{u} \mp \mathbf{v} \Delta t, t), \quad (6)$$

$$L(\mathbf{u} \mp \mathbf{v} \Delta t, t) = L(\mathbf{u}, t) \mp \nabla L(\mathbf{u}, t) \cdot \mathbf{v} \Delta t. \quad (7)$$

By applying Equation 7 on Equation 5, we have

$$\begin{aligned} \nabla L(\mathbf{u}, t \pm \Delta t) &= \nabla L(\mathbf{u}, t) \mp \nabla^2 L(\mathbf{u}, t) \cdot \mathbf{v} \Delta t, \\ \Delta L(\mathbf{u}, t \pm \Delta t) &= \Delta L(\mathbf{u}, t) \mp \mathbf{v} \cdot \nabla^2 L(\mathbf{u}, t) \cdot \mathbf{v} (\Delta t)^2, \end{aligned} \quad (8)$$

which indicates that in regions with constant velocity and illumination, the event accumulations are either monotone increasing or decreasing for a short period of time. Therefore, applying median filtering on voxels can preserve the accumulation values for temporally consistent regions while perturbing the values for other regions.

A.2. Network Level Protection

Noise Watermark Implementation In network level privacy protection, recall that we add noise watermarks to prevent the service provider from reverse engineering the newly trained network. Here a fixed noise watermark is assigned to each user re-training the event-to-image conversion network, and is unknown to the service provider. The noise watermark obfuscates the weights learned during the training process (Section 4.2) and thus prevents reverse engineering attacks (generic/targeted re-training). In all our experiments, we specifically set the noise watermark $E_{\text{noise}} \in \mathbb{R}^{B \times H \times W}$ as a voxel grid with each voxels randomly sampled from the normal distribution $\mathcal{N}(0, 1)$.

B. Experiment Details

B.1. Event Voxels for Image Conversion

In all our experiments we first package the input events to event voxel grids and apply event-to-image conversion methods [49, 57]. Given an event stream \mathcal{E} spanning ΔT seconds, the event voxel [49, 57, 75] is defined by taking weighted sums of event polarities within spatio-temporal bins. Formally, each entry of the event voxel $E \in \mathbb{R}^{B \times H \times W}$ is given as follows,

$$E(l, m, n) = \sum_{\substack{x_i=l \\ y_i=m}} p_i \max(0, 1 - |n - t_i^*|), \quad (10)$$

where $t_i^* = \frac{B-1}{\Delta T}(t_i - t_0)$ is the normalized event timestamp. Conventional event-to-image conversion methods [42, 49, 57, 63, 68] take the event voxels as input and produce image reconstructions using neural networks, namely $F_{\Theta}(E) = I$ where Θ denotes the neural network parameters. For all our experiments, we set the number of temporal bins for the event voxel as $B=50$, and the height and width is set as $H=180, W=240$ for the DAVIS240C [43] dataset and $H=260, W=346$ for the DAVIS346 [2] dataset. During the conversion, the E2VID [49] network processes 5 bins per inference and thus makes 10 repetitive inferences to obtain a single image from a stream of events.

B.2. Localization Evaluation

Query/Reference Split Here we explain how we prepare the query and reference set for evaluating localization. Recall from Section 3.1 that we build the 3D map from event-to-image conversions in the reference set and measure localization accuracy using the query set. For evaluation in EvRooms and DAVIS240C, we use the first 70% of the event streams for reference and the rest for querying. On the other hand for EvHumans, we randomly slice 70% of the event streams for reference and the rest for querying. The distinction is made for EvHumans because the dataset does not contain significant visual overlaps between the frontal and latter events as the capturing was made while constantly tracking the humans close by.

Baselines In Section 5.1 we consider six baselines for event-based visual localization: direct methods (PoseNet [30], SP-LSTM [46]), and structure-based methods taking various event representations as input (binary event image [11], event histogram [41, 69], timestamp image [47], and sorted timestamp image [6]). Following the implementation of Nguyen et al. [46], direct methods take the binary event image [11] as input which assigns +1 to pixels with positive events, 0 to pixels with negative events, and 0.5 otherwise. Both PoseNet [30] and SP-LSTM [46] are trained to directly regress the 6DoF pose within a scene, and needs to be re-trained for each scene. We train the networks separately for each scene in DAVIS240C [43], using the events in the reference split. Here the pose annotations from the 3D map built from image conversions are used to ensure that the network pose predictions are consistent with our method’s prediction. The networks are all trained for 1400 epochs using a batch size of 20 and a learning rate of $1e-4$ with Adam [34].

The structure-based methods are contrived baselines that omit the event-to-image conversion and directly package the input events for localization. Four conventional packaging methods are tested including the binary event image, with event histograms [41, 69] caching the pixel-wise event counts, timestamp image [47] caching the pixel-wise most recent event timestamps, and sorted timestamp image [6] caching the relative order of timestamps instead of the raw values. We use the poses from the 3D maps built from event-to-image conversions, but replace the images to corresponding event representations during localization.

B.3. Sensor Level Privacy Protection

Group Re-Identification Task In Section 5.2 we introduce the group re-identification task, to evaluate how the sensor level privacy protection can affect the high-level facial semantics. Here we explain the detailed evaluation process for this task. Prior to evaluation, we first run face de-

Method	t -error	R -error	Acc.	# of Faces	Sharpness	Re-ID Acc.
No Filtering	0.04	0.99	0.84	1034	0.0956	0.9387
Gaussian Filtering	0.11	2.85	0.42	55	0.0341	0.4151
Mean Filtering	0.04	1.12	0.77	372	0.0449	0.5755
Ours	0.05	1.28	0.73	192	0.0475	0.5377

Table B.1. Privacy protection comparison against simple filtering methods.

tection [3] on the non-filtered image reconstructions and obtain the bounding boxes for the detected faces. We use the bounding boxes to crop facial regions in the filtered image reconstructions similar to the image sharpness evaluation in Section 5.2.1.

For each scene from EvHumans, we make two groups with the first group \mathcal{G}_{in} containing the faces of all the people appearing in the scene and the second group \mathcal{G}_{out} containing the faces of the remaining people. Then we further split \mathcal{G}_{in} into two groups $\mathcal{G}_{in}^{ref}, \mathcal{G}_{in}^{test}$ with \mathcal{G}_{in}^{ref} containing the first 80% of the faces and \mathcal{G}_{in}^{test} containing the rest. Finally, for each face in \mathcal{G}_{in}^{test} we (i) extract the ArcFace [13] descriptor and compare against the descriptors extracted for faces in \mathcal{G}_{in}^{ref} and \mathcal{G}_{out} , and (ii) choose the group with the smallest L2 descriptor distance. The accuracy in Table 2 from Section 5.2 is measured as the ratio of predictions with the correct group predictions.

Comparison against Gaussian and Mean Filtering We make comparisons against more simpler design choices for voxel filtering, namely Gaussian and mean filtering. The filtering operations are performed with a spatio-temporal kernel size of $5 \times 5 \times 5$, and the blending operations is kept identically as our sensor level protection method. The results are summarized in Table B.1. Gaussian filtering results in harsher removal of feature points and incurs large drop in localization accuracy. Mean filtering on the other hand shows smaller localization performance drop but fails in protecting facial information which could be indicated from the large number of face detections. Our method better balances between privacy protection and localization performance preservation.

B.4. Network Level Privacy Protection

Image Similarity Metrics We describe the metrics for evaluating privacy protection against possible attacks from the service provider. Recall that we measure the similarity between the attack results and the original event-to-image reconstruction using MAE, PSNR, and SSIM. First, given the attack result I_{atk} and ground-truth image I , mean absolute error (MAE) is defined as follows,

$$MAE(I, I_{atk}) = |I - I_{atk}|. \quad (11)$$

In addition, PSNR is given as follows,

$$\text{PSNR}(I, I_{\text{atk}}) = 20 \cdot \log_{10}(\text{MAX}_I) - 10 \cdot \log_{10}(\text{MSE}), \quad (12)$$

where MAX_I is the maximum possible pixel value of the image and MSE is the mean squared error. Unlike the other two metrics, SSIM is first defined for a pair of $N \times N$ windows x and y as follows,

$$\text{SSIM}_{\text{patch}}(x, y) = \frac{(2\mu_x\mu_y + c_1)(2\sigma_{xy} + c_2)}{(\mu_x^2 + \mu_y^2 + c_1)(\sigma_x^2 + \sigma_y^2 + c_2)}, \quad (13)$$

where μ_x, μ_y are the mean value of the windows, σ_x, σ_y are the standard deviation of the windows, σ_{xy} is the covariance between the windows, and $c_1 = 6.5025, c_2 = 58.5225$. Then the total SSIM value is given as the patch-wise averages, namely,

$$\text{SSIM}(I, I_{\text{atk}}) = \frac{1}{|X||Y|} \sum_{x,y} \text{SSIM}_{\text{patch}}(x, y), \quad (14)$$

where $|X|, |Y|$ are the total number of patches in I and I_{atk} respectively. In all our experiments, we used SSIM with a window size of $N = 11$.

Evaluation Protocol We elaborate on the detailed procedures for evaluating network level privacy protection. Recall that to hide the entire user’s view from service providers in private scenes, we propose to re-train the neural networks and distribute the inference between the user and service provider. The evaluation process is summarized in Figure B.1. We use the 6 scenes from DAVIS240C [43] as in Section 5.1 and first train a new set of event-to-image conversion networks for each scene. Here we train each conversion network using the events from the reference set described in Section B.2. Then, we train the conversion networks for generic and targeted re-training using 3,000 event sequences each spanning 2 seconds generated from the MSCOCO dataset [40] following [49, 57]. Finally, to make attacks for each scene we apply swapped layer inference using (i) the original network weights Θ , (ii) the generic re-training weights, and (iii) the targeted re-training weights. Note that for results in the main paper we refer to the first case as swapped layer inference, the second case as generic re-training, and the third case as targeted re-training.

Full Privacy Protection Evaluation Results We report the entire evaluation results measured at various neural network locations for swapped layer inference. Namely, similar to Figure B.1b we experiment swapping the network layers after (i) the first two layers, (ii) the first three layers, (iii) the first six layers, and (iv) the entire middle part F_{Θ}^2 . Table B.2 reports the results for additional image similarity metrics (PSNR, SSIM), where the results for mean

Attack Type	Swapped Layer Inference	Generic Re-Training	Targeted Re-Training
Random Initialization	11.5582	11.5904	17.8546
Ours w/o Noise Watermark	5.6959	12.2696	15.0348
Ours w/o Adversarial Loss	11.1425	11.7435	14.0036
Ours	6.184	11.9569	11.8629

(a) Reconstruction Quality (PSNR) of Possible Attacks

Attack Type	Swapped Layer Inference	Generic Re-Training	Targeted Re-Training
Random Initialization	0.0302	0.0460	0.3743
Ours w/o Noise Watermark	0.0247	0.0536	0.2223
Ours w/o Adversarial Loss	0.0067	0.0226	0.0783
Ours	0.0327	0.0539	0.0527

(b) Reconstruction Quality (SSIM) of Possible Attacks

Table B.2. Network level privacy preservation evaluation on additional image similarity metrics.

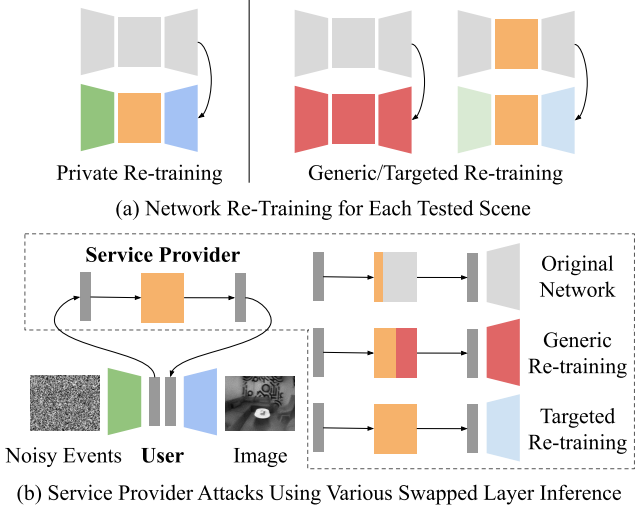


Figure B.1. Evaluation procedure of network level privacy protection. For each tested scene, we first train a new set of neural networks in the user side and apply generic/targeted re-training in the service provider side. Then to evaluate the possible attacks we perform swapped layer inference using the three types of network weights available to the service provider (original, generic re-training, targeted re-training) at various network swapping locations.

absolute error (MAE) are reported in Table 4 from Section 5.2. Due to the noise watermark and adversarial loss, our network level protection can robustly defend against all the considered attacks.

B.5. User Study

User Comments To evaluate how the general public feels about our privacy protection methods, we conduct a user study with 39 participants. Along with the insecurity scoring mentioned in Section 5.2, we requested the users to op-

“I don't think there's a need to hide information other than face information during the pre-processing.”

“With this preprocessing, it's hard to distinguish the silhouettes of people, therefore less concerning in the perspective of privacy.”

“The reconstructed images absolutely hide the sensitive details.”

“I think people cannot recognize my facial information after pre-processing takes place.”

“I would feel less insecure with pre-processing since it blurs out the facial details to the point where individuals are hardly verifiable.”

“It might be possible to identify someone by his/her unique body features or personal habits.”

“It can be dangerous if one can reverse the pre-processing, or try to track someone using gait and gesture information.”

Figure B.2. Positive and negative comments from the user study about our privacy protection method.

tionally leave comments about their evaluations. We share the user comments in Figure B.2. Overall, the positive comments emphasize the fact that for sensor level protection the facial details are sufficiently removed and for network level protection the reconstructions successfully hide the entire user’s view. Nevertheless, there were some negative comments about the sensor level protection that other signals such as unique gestures or body features are not obscured. Devising a privacy protection method that can cover a wider range of biometric signals is left as future work.

Survey Details As mentioned in Section 5.2, we first ask the users about how insecure they feel in various capturing scenarios using normal cameras. Then we show event visualizations along with images, where the users are asked again to make an insecurity assessment. Finally for assessing our privacy protection methods, we show the event-to-image conversion results, followed by our privacy protection results and request another set of insecurity assessment. Note that we showed multiple videos for each scenario in the actual user study, and for sensor level evaluation we additionally showed samples of faces reconstructed after processing.

B.6. Additional Qualitative Results and Video

In Figure B.3 we display additional qualitative samples for sensor level and network level protection. Our privacy protection methods can effectively hide sensitive visual details, enabling privacy-preserving event-based visual localization.

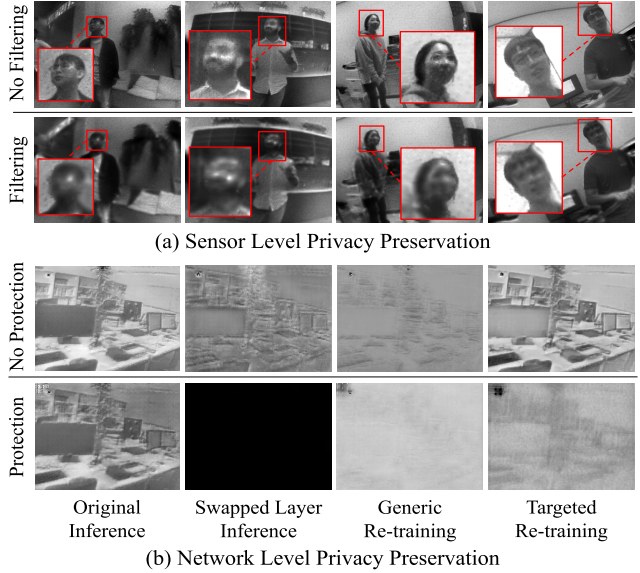


Figure B.3. Additional qualitative results of privacy protection.

C. Dataset Details

DAVIS240C We use six scenes from DAVIS240C [43] for localization evaluation in Section 5. Specifically, we use `dynamic_6DoF`, `poster_6DoF`, `boxes_6DoF`, `hdr_boxes`, `hdr_poster`, and `office_zigzag` for evaluation. Among these scenes `hdr_boxes` and `hdr_poster` are recorded under low light conditions.

EvRooms We collect EvRooms using the DAVIS346 camera [2] from 19 scenes, with 7 scenes additionally recorded under low lighting. Some exemplary 3D structure-from-motion (SfM) maps and images are shown in Figure C.4. As explained in Section 3, we obtain the 3D maps by first converting short event streams to images [49] and using an off-the-shelf 3D reconstruction software COLMAP [58]. The dataset contains pose annotations for 18323 images converted from events in fast camera motion (EvRooms^F), along with 5022 images for events captured in low lighting (EvRooms^L). For localization evaluation in Section 5.1, we set the Normal split as the four scenes in DAVIS240C (`dynamic_6DoF`, `poster_6DoF`, `boxes_6DoF`, `office_zigzag`). To evaluate localization in more challenging scenarios, we set the Low Lighting split as the two scenes in DAVIS240C (`hdr_boxes`, `hdr_poster`) along with EvRooms^L, and the Fast Motion split as the scenes in EvRooms^F. We are planning to partially release the EvRooms dataset in public.

EvHumans For evaluating localization amidst moving people, we use the newly captured dataset called EvHumans. Similar to EvRooms, this dataset was captured us-

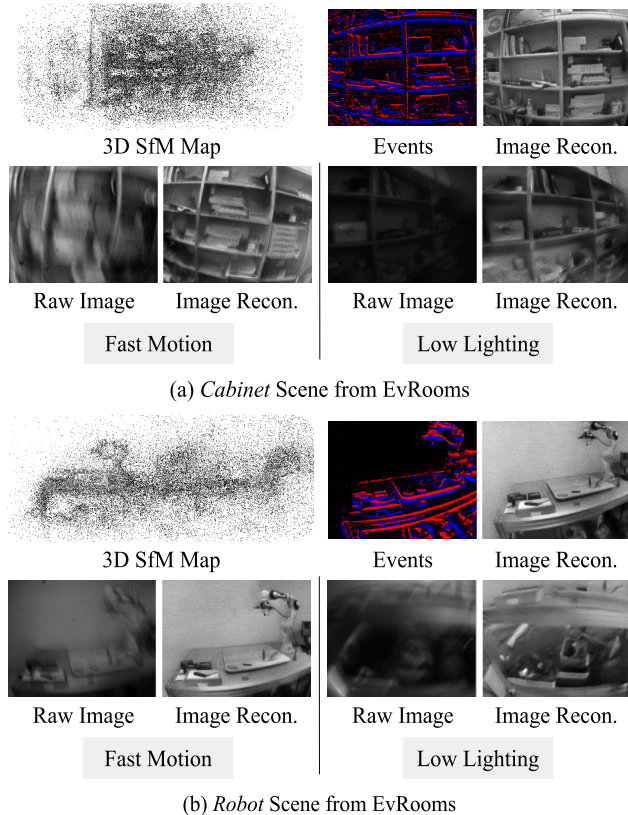


Figure C.4. Visualization of 3D maps, events, images, and event-to-image conversions from EvRooms. While the dataset contains challenging scenarios such as fast camera motion or low lighting, event cameras offer stable visual cues for robust localization.

ing the DAVIS346 camera [2] and we obtain the 3D maps using the event-to-image conversions with COLMAP [58]. The dataset consists of 20 scenes with 16 volunteers, where each scene on average contains 2~3 moving people. Prior to dataset capture, we obtained the consent from all 16 volunteers under the conditions that the dataset is not made public. We additionally obtained approval from the volunteers whose faces appear in the paper figures. Note that none of the authors' faces are present in the figures to abide by the double-blind policy.

References

- [1] Capturing snaps-spectacles support. <https://support.spectacles.com/hc/en-us/articles/360000439746-Capturing-Snaps>. Accessed: 2022-11-09. 2
- [2] Davis 346 camera. <https://shop.inivation.com/products/davis346>. Accessed: 2022-11-01. 5, 9, 12, 13
- [3] Facenet-pytorch. <https://github.com/timesler/facenet-pytorch>. Accessed: 2022-11-01. 6, 10
- [4] Japan's noisy iphone problem. <https://www.engadget.com/2016-09-30-japans-noisy-iphone-problem.html>. Accessed: 2022-11-09. 2
- [5] Meta quest pro. <https://www.meta.com/kr/en/quest/quest-pro/>. Accessed: 2022-11-09. 2
- [6] I. Alzugaray and M. Chli. Ace: An efficient asynchronous corner tracker for event cameras. In *2018 International Conference on 3D Vision (3DV)*, pages 653–661, 2018. 6, 10
- [7] R. Arandjelović, P. Gronat, A. Torii, T. Pajdla, and J. Sivic. NetVLAD: CNN architecture for weakly supervised place recognition. In *IEEE Conference on Computer Vision and Pattern Recognition*, 2016. 2, 3, 6
- [8] C. Brandli, R. Berner, M. Yang, S. Liu, and T. Delbruck. A 240 × 180 130 db 3 μs latency global shutter spatiotemporal vision sensor. *IEEE Journal of Solid-State Circuits*, 49(10):2333–2341, 2014. 5
- [9] Samuel Bryner, Guillermo Gallego, Henri Rebecq, and Davide Scaramuzza. Event-based, direct camera tracking from a photometric 3d map using nonlinear optimization. In *2019 International Conference on Robotics and Automation (ICRA)*, pages 325–331, 2019. 2
- [10] Christian Cachin, Idit Keidar, and Alexander Shraer. Trusting the cloud. *SIGACT News*, 40(2):81–86, jun 2009. 1, 2
- [11] G. Cohen, S. Afshar, G. Orchard, J. Tapson, R. Benosman, and A. van Schaik. Spatial and temporal downsampling in event-based visual classification. *IEEE Transactions on Neural Networks and Learning Systems*, 29(10):5030–5044, 2018. 5, 6, 10
- [12] Deeksha Dangwal, Vincent T. Lee, Hyo Jin Kim, Tianwei Shen, Meghan Cowan, Rajvi Shah, Caroline Trippel, Brandon Reagan, Timothy Sherwood, Vasileios Balntas, Armin Alaghi, and Eddy Ilg. Analysis and mitigations of reverse engineering attacks on local feature descriptors, 2021. 1, 2, 3, 8
- [13] Jiankang Deng, Jia Guo, Niannan Xue, and Stefanos Zafeiriou. Arcface: Additive angular margin loss for deep face recognition. In *Proceedings of the IEEE/CVF Conference on Computer Vision and Pattern Recognition (CVPR)*, June 2019. 7, 10
- [14] Daniel DeTone, Tomasz Malisiewicz, and Andrew Rabinovich. Superpoint: Self-supervised interest point detection and description. In *CVPR Deep Learning for Visual SLAM Workshop*, 2018. 2, 3, 6
- [15] Mihai Dusmanu, Johannes Schönberger, Sudipta Sinha, and Marc Pollefeys. Privacy-preserving image features via adversarial affine subspace embeddings. In *Computer Vision and Pattern Recognition (CVPR 2021)*. CVF/IEEE, June 2021. 3, 4, 8
- [16] Zekeriya Erkin, Martin Franz, Jorge Guajardo, Stefan Katzenbeisser, Inald Lagendijk, and Tomas Toft. Privacy-preserving face recognition. In Ian Goldberg and Mikhail J. Atallah, editors, *Privacy Enhancing Technologies*, pages 235–253, Berlin, Heidelberg, 2009. Springer Berlin Heidelberg. 2
- [17] Tobias Fischer and Michael Milford. Event-based visual place recognition with ensembles of temporal windows. *IEEE Robotics and Automation Letters*, 5(4):6924–6931, 2020. 5

- [18] Martin A. Fischler and Robert C. Bolles. Random sample consensus: A paradigm for model fitting with applications to image analysis and automated cartography. *Commun. ACM*, 24(6):381–395, 1981. [3](#), [6](#)
- [19] G. Gallego, T. Delbrück, G. Orchard, C. Bartolozzi, B. Taba, A. Censi, S. Leutenegger, A. Davison, J. Conradt, Kostas Daniilidis, and D. Scaramuzza. Event-based vision: A survey. *IEEE transactions on pattern analysis and machine intelligence*, PP, 2020. [2](#), [9](#)
- [20] Guillermo Gallego, Jon E.A. Lund, Elias Mueggler, Henri Rebecq, Tobi Delbruck, and Davide Scaramuzza. Event-based, 6-dof camera tracking from photometric depth maps. *IEEE Transactions on Pattern Analysis and Machine Intelligence*, 40(10):2402–2412, 2018. [2](#)
- [21] Marcel Geppert, Viktor Larsson, Pablo Speciale, Johannes L. Schönberger, and Marc Pollefeys. Privacy preserving structure-from-motion. 2020. [3](#)
- [22] J. A. Hesch and S. I. Roumeliotis. A direct least-squares (dls) method for pnp. In *2011 International Conference on Computer Vision*, pages 383–390, 2011. [3](#)
- [23] Javier Hidalgo-Carrió, Guillermo Gallego, and Davide Scaramuzza. Event-aided direct sparse odometry. In *Proceedings of the IEEE Conference on Computer Vision and Pattern Recognition (CVPR)*, June 2022. [2](#)
- [24] Martin Humenberger, Yohann Cabon, Nicolas Guerin, Julien Morat, Jérôme Revaud, Philippe Rerole, Noé Pion, Cesar de Souza, Vincent Leroy, and Gabriela Csurka. Robust image retrieval-based visual localization using kapture, 2020. [2](#)
- [25] Martin Humenberger, Yohann Cabon, Nicolas Guerin, Julien Morat, Jérôme Revaud, Philippe Rerole, Noé Pion, Cesar de Souza, Vincent Leroy, and Gabriela Csurka. Robust image retrieval-based visual localization using kapture, 2020. [2](#)
- [26] Inwoo Hwang, Junho Kim, and Young Min Kim. Ev-nerf: Event based neural radiance field. In *Proceedings of the IEEE/CVF Winter Conference on Applications of Computer Vision (WACV)*, January 2023. [2](#)
- [27] Jianhao Jiao, Huaiyang Huang, Liang Li, Zhijian He, Yilong Zhu, and Ming Liu. Comparing representations in tracking for event camera-based SLAM. *CoRR*, abs/2104.09887, 2021. [2](#)
- [28] Yifan Jin, Lei Yu, Guangqiang Li, and Shumin Fei. A 6-dofs event-based camera relocation system by cnn-lstm and image denoising. *Expert Systems with Applications*, 170:114535, 2021. [2](#)
- [29] Nick Kanopoulos, Nagesh Vasanthavada, and Robert L. Baker. Design of an image edge detection filter using the sobel operator. *IEEE Journal of solid-state circuits*, 23(2):358–367, 1988. [5](#)
- [30] Alex Kendall, Matthew Grimes, and Roberto Cipolla. Posenet: A convolutional network for real-time 6-dof camera relocation. 2015. [2](#), [5](#), [6](#), [10](#)
- [31] Hanme Kim, Ankur Handa, Ryad Benosman, Sio-Hoi Ieng, and Andrew Davison. Simultaneous mosaicing and tracking with an event camera. In *Proceedings of the British Machine Vision Conference*. BMVA Press, 2014. [2](#)
- [32] Hanme Kim, Stefan Leutenegger, and Andrew J. Davison. Real-time 3d reconstruction and 6-dof tracking with an event camera. In *ECCV*, 2016. [2](#)
- [33] Junho Kim, Changwoon Choi, Hojun Jang, and Young Min Kim. Piccolo: Point cloud-centric omnidirectional localization. In *Proceedings of the IEEE/CVF International Conference on Computer Vision (ICCV)*, pages 3313–3323, October 2021. [5](#)
- [34] Diederik P. Kingma and Jimmy Ba. Adam: A method for stochastic optimization. In Yoshua Bengio and Yann LeCun, editors, *3rd International Conference on Learning Representations, ICLR 2015, San Diego, CA, USA, May 7-9, 2015, Conference Track Proceedings*, 2015. [7](#), [10](#)
- [35] Simon Klenk, Lukas Koestler, Davide Scaramuzza, and Daniel Cremers. E-nerf: Neural radiance fields from a moving event camera, 2022. [2](#)
- [36] Sudhakar Kumawat and Hajime Nagahara. Privacy-preserving action recognition via motion difference quantization. In *Proceedings of the European Conference on Computer Vision (ECCV)*, October 2022. [2](#)
- [37] Vincent Lepetit, Francesc Moreno-Noguer, and Pascal Fua. Epanp: An accurate o(n) solution to the pnp problem. *Int. J. Comput. Vision*, 81(2):155–166, Feb. 2009. [3](#)
- [38] Vincent Lepetit, Francesc Moreno-Noguer, and Pascal Fua. Epanp: An accurate o(n) solution to the pnp problem. *International Journal Of Computer Vision*, 81:155–166, 2009. [3](#), [6](#)
- [39] Patrick Lichtsteiner, Christoph Posch, and Tobi Delbruck. A 128× 128 120 db 15 μ s latency asynchronous temporal contrast vision sensor. *IEEE Journal of Solid-State Circuits*, 43(2):566–576, 2008. [2](#)
- [40] Tsung-Yi Lin, Michael Maire, Serge Belongie, James Hays, Pietro Perona, Deva Ramanan, Piotr Dollár, and C. Lawrence Zitnick. Microsoft coco: Common objects in context. In David Fleet, Tomas Pajdla, Bernt Schiele, and Tinne Tuytelaars, editors, *Computer Vision – ECCV 2014*, pages 740–755, Cham, 2014. Springer International Publishing. [7](#), [11](#)
- [41] Ana I. Maqueda, Antonio Loquercio, G. Gallego, N. García, and D. Scaramuzza. Event-based vision meets deep learning on steering prediction for self-driving cars. *2018 IEEE/CVF Conference on Computer Vision and Pattern Recognition*, pages 5419–5427, 2018. [6](#), [10](#)
- [42] Nico Messikommer, Daniel Gehrig, Antonio Loquercio, and Davide Scaramuzza. Learning to see in the dark with events. 2020. [3](#), [9](#)
- [43] Elias Mueggler, Henri Rebecq, Guillermo Gallego, Tobi Delbruck, and Davide Scaramuzza. The event-camera dataset and simulator: Event-based data for pose estimation, visual odometry, and slam. *The International Journal of Robotics Research*, 36(2):142–149, 2017. [5](#), [9](#), [10](#), [11](#), [12](#)
- [44] Manasi Muglikar, Mathias Gehrig, Daniel Gehrig, and Davide Scaramuzza. How to calibrate your event camera. In *IEEE Conf. Comput. Vis. Pattern Recog. Workshops (CVPRW)*, June 2021. [5](#)
- [45] Tony Ng, Hyo Jin Kim, Vincent T. Lee, Daniel DeTone, Tsun-Yi Yang, Tianwei Shen, Eddy Ilg, Vassileios Balntas, Krystian Mikolajczyk, and Chris Sweeney. Ninjadesc: Content-concealing visual descriptors via adversarial learning. In *Proceedings of the IEEE/CVF Conference on Computer Vision and Pattern Recognition (CVPR)*, pages 12797–12807, June 2022. [3](#), [4](#), [8](#)

- [46] Anh Nguyen, Thanh-Toan Do, Darwin G. Caldwell, and Nikos G. Tsagarakis. Real-time 6dof pose relocation for event cameras with stacked spatial lstm networks. In *2019 IEEE/CVF Conference on Computer Vision and Pattern Recognition Workshops (CVPRW)*, pages 1638–1645, 2019. 2, 5, 6, 10
- [47] P. K. J. Park, B. H. Cho, J. M. Park, K. Lee, H. Y. Kim, H. A. Kang, H. G. Lee, J. Woo, Y. Roh, W. J. Lee, C. Shin, Q. Wang, and H. Ryu. Performance improvement of deep learning based gesture recognition using spatiotemporal demosaicing technique. In *2016 IEEE International Conference on Image Processing (ICIP)*, pages 1624–1628, 2016. 6, 10
- [48] Francesco Pittaluga and Sanjeev J. Koppal. Privacy preserving optics for miniature vision sensors. In *2015 IEEE Conference on Computer Vision and Pattern Recognition (CVPR)*, pages 314–324, 2015. 2
- [49] H. Rebecq, R. Ranftl, V. Koltun, and D. Scaramuzza. Events-to-video: Bringing modern computer vision to event cameras. In *2019 IEEE/CVF Conference on Computer Vision and Pattern Recognition (CVPR)*, pages 3852–3861, 2019. 2, 3, 5, 8, 9, 11, 12
- [50] Viktor Rudnev, Mohamed Elgharib, Christian Theobalt, and Vladislav Golyanik. Eventnerf: Neural radiance fields from a single colour event camera, 2022. 2
- [51] Paul-Edouard Sarlin, Cesar Cadena, Roland Siegwart, and Marcin Dymczyk. From coarse to fine: Robust hierarchical localization at large scale. In *CVPR*, 2019. 2, 5
- [52] Paul-Edouard Sarlin, Daniel DeTone, Tomasz Malisiewicz, and Andrew Rabinovich. SuperGlue: Learning feature matching with graph neural networks. In *CVPR*, 2020. 2, 3
- [53] Torsten Sattler, Bastian Leibe, and Leif Kobbelt. Efficient & effective prioritized matching for large-scale image-based localization. *IEEE Trans. Pattern Anal. Mach. Intell.*, 39(9):1744–1756, 2017. 2, 5
- [54] Torsten Sattler, Will Maddern, Carl Toft, Akihiko Torii, Lars Hammarstrand, Erik Stenborg, Daniel Safari, Masatoshi Okutomi, Marc Pollefeys, Josef Sivic, Fredrik Kahl, and Tomas Pajdla. Benchmarking 6DOF Outdoor Visual Localization in Changing Conditions. In *Conference on Computer Vision and Pattern Recognition (CVPR)*, 2018. 1
- [55] T. Sattler, Q. Zhou, M. Pollefeys, and L. Leal-Taixe. Understanding the limitations of cnn-based absolute camera pose regression. In *2019 IEEE/CVF Conference on Computer Vision and Pattern Recognition (CVPR)*, pages 3297–3307, Los Alamitos, CA, USA, jun 2019. IEEE Computer Society. 2
- [56] Cedric Scheerlinck, Nick Barnes, and Robert Mahony. Continuous-time intensity estimation using event cameras. In C.V. Jawahar, Hongdong Li, Greg Mori, and Konrad Schindler, editors, *Computer Vision – ACCV 2018*, pages 308–324, Cham, 2019. Springer International Publishing. 2
- [57] Cedric Scheerlinck, Henri Rebecq, Daniel Gehrig, Nick Barnes, Robert E. Mahony, and Davide Scaramuzza. Fast image reconstruction with an event camera. In *2020 IEEE Winter Conference on Applications of Computer Vision (WACV)*, pages 156–163, 2020. 2, 3, 8, 9, 11
- [58] Johannes Lutz Schönberger and Jan-Michael Frahm. Structure-from-motion revisited. In *Conference on Computer Vision and Pattern Recognition (CVPR)*, 2016. 3, 12, 13
- [59] Sefik Ilkin Serengil and Alper Ozpinar. Lightface: A hybrid deep face recognition framework. In *2020 Innovations in Intelligent Systems and Applications Conference (ASYU)*, pages 23–27. IEEE, 2020. 6
- [60] Sefik Ilkin Serengil and Alper Ozpinar. Hyperextended lightface: A facial attribute analysis framework. In *2021 International Conference on Engineering and Emerging Technologies (ICEET)*, pages 1–4. IEEE, 2021. 6
- [61] Pablo Speciale, Johannes L. Schönberger, Sing Bing Kang, Sudipta N. Sinha, and Marc Pollefeys. Privacy preserving image-based localization. 2019. 3, 4, 8
- [62] Pablo Speciale, Johannes Schönberger, Sudipta Sinha, and Marc Pollefeys. Privacy preserving image queries for camera localization. In *2019 IEEE/CVF International Conference on Computer Vision (ICCV)*, pages 1486–1496, 2019. 3, 4, 8
- [63] T. Stoffregen, C. Scheerlinck, D. Scaramuzza, T. Drummond, N. Barnes, L. Kleeman, and R. Mahoney. Reducing the sim-to-real gap for event cameras. In *European Conference on Computer Vision (ECCV)*, august 2020. 2, 3, 9
- [64] Hajime Taira, Masatoshi Okutomi, Torsten Sattler, Mircea Cimpoi, Marc Pollefeys, Josef Sivic, Tomas Pajdla, and Akihiko Torii. InLoc: Indoor Visual Localization with Dense Matching and View Synthesis. In *CVPR 2018 - IEEE Conference on Computer Vision and Pattern Recognition*, Salt Lake City, United States, June 2018. 1
- [65] Jasper Tan, Salman S. Khan, Vivek Boominathan, Jeffrey Byrne, Richard Baraniuk, Kaushik Mitra, and Ashok Veeraraghavan. Canopic: Pre-digital privacy-enhancing encodings for computer vision. In *2020 IEEE International Conference on Multimedia and Expo (ICME)*, pages 1–6, 2020. 2
- [66] Zaid Tasneem, Giovanni Milione, Yi-Hsuan Tsai, Xiang Yu, Ashok Veeraraghavan, Chandraker Manmohan, and Francesco Pittaluga. Learning phase mask for privacy-preserving passive depth estimation. In *Proceedings of the European Conference on Computer Vision (ECCV)*, October 2022. 2
- [67] Florian Walch, Caner Hazirbas, Laura Leal-Taixe, Torsten Sattler, Sebastian Hilsenbeck, and Daniel Cremers. Image-based localization using lstms for structured feature correlation. In *Proceedings of the IEEE International Conference on Computer Vision (ICCV)*, Oct 2017. 1, 2
- [68] L. Wang, I. S. M. Mostafavi, Y. Ho, and K. Yoon. Event-based high dynamic range image and very high frame rate video generation using conditional generative adversarial networks. In *2019 IEEE/CVF Conference on Computer Vision and Pattern Recognition (CVPR)*, pages 10073–10082, 2019. 2, 3, 9
- [69] Y. Wang, B. Du, Y. Shen, K. Wu, G. Zhao, J. Sun, and H. Wen. Ev-gait: Event-based robust gait recognition using dynamic vision sensors. In *2019 IEEE/CVF Conference on Computer Vision and Pattern Recognition (CVPR)*, pages 6351–6360, 2019. 6, 10

- [70] Yinggui Wang, Jian Liu, Man Luo, Le Yang, and Li Wang. Privacy-preserving face recognition in the frequency domain. *Proceedings of the AAAI Conference on Artificial Intelligence*, 36(3):2558–2566, June 2022. [2](#)
- [71] P. Wenzel, R. Wang, N. Yang, Q. Cheng, Q. Khan, L. von Stumberg, N. Zeller, and D. Cremers. 4Seasons: A cross-season dataset for multi-weather SLAM in autonomous driving. In *Proceedings of the German Conference on Pattern Recognition (GCPR)*, 2020. [1](#)
- [72] Thomas Winkler, Ádám Erdélyi, and Bernhard Rinner. Trusteye.m4: Protecting the sensor — not the camera. In *2014 11th IEEE International Conference on Advanced Video and Signal Based Surveillance (AVSS)*, pages 159–164, 2014. [2](#)
- [73] Jia Xiang and Gengming Zhu. Joint face detection and facial expression recognition with mtcnn. In *2017 4th International Conference on Information Science and Control Engineering (ICISCE)*, pages 424–427, 2017. [7](#)
- [74] Richard Zhang, Phillip Isola, Alexei A Efros, Eli Shechtman, and Oliver Wang. The unreasonable effectiveness of deep features as a perceptual metric. In *CVPR*, 2018. [5](#)
- [75] Alex Zihao Zhu, Liangzhe Yuan, Kenneth Chaney, and Kostas Daniilidis. Unsupervised event-based optical flow using motion compensation. In Laura Leal-Taixé and Stefan Roth, editors, *Computer Vision – ECCV 2018 Workshops*, pages 711–714, Cham, 2019. Springer International Publishing. [3](#), [9](#)